Uncertainty in the response of sudden stratospheric warmings and stratosphere-troposphere coupling to quadrupled CO2 concentrations in CMIP6 models

B. Ayarzagüena[1], A. J. Charlton-Perez[2], A. H. Butler[3], P. Hitchcock[4], I. R. Simpson[5], L. M. Polvani[6], N. Butchart[7], E. P. Gerber[8], L. Gray[9], B. Hassler[10], P. Lin[11], F. Lott[12], E. Manzini[13], R. Mizuta[14], C. Orbe[15], S. Osprey[9], D. Saint-Martin[16], M. Sigmond[17], M. Taguchi[18], E. M. Volodin[19], S. Watanabe[20]

[1] Departamento de Física de la Tierra y Astrofísica, Universidad Complutense de Madrid, Spain

[2] Department of Meteorology, Univ. of Reading, UK

[3] Cooperative Institute for Environmental Sciences (CIRES)/National Oceanic and Atmospheric Administration (NOAA) Chemical Sciences Division, USA

[4] Department of Earth and Atmospheric Sciences, Cornell University, USA

[5] Climate and Global Dynamics Laboratory, National Center for Atmospheric Research, USA

[6] Columbia University, USA

[7] Met Office Hadley Centre, Exeter, UK.

[8] Courant Institute of Mathematical Sciences, New York University, USA

[9] NCAS-Climate, Department of Physics, University of Oxford, UK

[10] Deutsches Zentrum für Luft-und Raumfahrt (DLR), Oberpfaffenhofen, Germany

[11] Atmospheric and Oceanic Sciences Program, Princeton University, USA,

[12] Laboratoire de Météorologie Dynamique, Ecole Normale Supérieure, France

[13] Max-Planck-Institut für Meteorologie, Germany

[14] Meteorological Research Institute, Japan

[15] NASA Goddard Institute for Space Studies, USA

[16] Centre National de Recherches Météorologiques (CNRM), Université de Toulouse, Météo-France, CNRS, Toulouse, France

[17] Canadian Centre for Climate Modelling and Analysis Environment and Climate Change, Canada

[18] Department of Earth Science, Aichi University of Education, Kariya, Japan

[19] Marchuk Institute of Numerical Mathematics, Russia

[20] Japan Agency for Marine-Earth Science and Technology (JAMSTEC), Japan

Corresponding author: Blanca Ayarzagüena (bayarzag@ucm.es)

Key Points:

- The tropospheric signal of Sudden Stratospheric Warming (SSWs) in the North Atlantic does not change under 4xCO_2 forcing.
- There is high uncertainty in changes of SSW frequency under 4xCO_2 forcing; single models show the rate to be significantly halved or doubled.
- The boreal polar vortex will form earlier and disappear later under increased CO_2, extending the season of stratosphere-troposphere coupling.

Abstract

Major sudden stratospheric warmings (SSWs), vortex formation and final breakdown dates are key highlight points of the stratospheric polar vortex. These phenomena are relevant for stratosphere-troposphere coupling, which explains the interest in understanding their future changes. However, up to now, there is not a clear consensus on which projected changes to the polar vortex are robust, particularly in the Northern Hemisphere, possibly due to short data record or relatively moderate CO_2 forcing. The new simulations performed under the Coupled Model Intercomparison Project, Phase 6, together with the long daily data requirements of the DynVarMIP project in preindustrial and quadrupled CO_2 ($4xCO_2$) forcing simulations provide a new opportunity to revisit this topic by overcoming the limitations mentioned above.

In this study, we analyze this new model output to document the change, if any, in the frequency of SSWs under $4xCO_2$ forcing. Our analysis reveals a large disagreement across the models as to the sign of this change, even though most models show a statistically significant change. The models, however, are in good agreement as to the impact of SSWs over the North Atlantic: there is no indication of a change under $4xCO_2$ forcing. Over the Pacific, however, the change is more uncertain. Finally, the models show robust changes to the seasonal cycle in the stratosphere. Specifically, we find a longer duration of the stratospheric polar vortex, and thus a longer season of stratosphere-troposphere coupling.

1 Introduction

The stratospheric polar vortex is a strong wintertime circumpolar cyclonic circulation that isolates the polar air masses from air in the lower latitudes [Andrews et al. 1987]. The stratospheric polar vortex forms in Autumn as solar heating vanishes at the pole, establishing strong meridional temperature gradients. The vortex intensifies during winter and then decays in spring as sunlight returns to high latitudes. The springtime breakdown of the vortex, when the zonal winds revert to easterlies, is also known as the stratospheric final warming (SFW).

Interest in the polar vortex has increased in the last decades for two different reasons. First, the magnitude of the Antarctic ozone hole is dependent on the state of the polar vortex, as a strong polar vortex is associated with colder temperatures (crucial for heterogeneous ozone chemistry) and reduced mixing with ozone-rich mid-latitude air [Schoeberl and Hartmann, 1991]. Secondly, polar stratospheric variability is known to affect not only the stratosphere but also the troposphere, typically projecting onto Annular Mode patterns [e.g.: Baldwin and Dunkerton, 2001; Kidston et al., 2015]. Polar stratospheric variability peaks in the winter hemisphere when the polar vortex is present, as a major source of stratospheric variability is upward propagating, planetary-scale Rossby waves from the troposphere below [Charney and Drazin, 1961]. Under linear theory, the vertical propagation of Rossby waves is limited to regions with westerly winds [Andrews et al. 1987]. Furthermore, because wave activity is greater in the Northern Hemisphere (NH) than in the Southern Hemisphere (SH) so is the polar stratospheric variability. In the SH, stratospheric variability, and thus the coupling to the troposphere, is mainly associated with SFW [Black and McDaniel 2007]. In the NH apart from SFWs [Black et al. 2006; Ayarzagüena and Serrano, 2009; Hardiman et al., 2011], this coupling is primarily associated with polar vortex extremes, in particular, major sudden stratospheric warmings (SSWs). SSWs happen in midwinter and consist in a reversal of wintertime polar stratospheric circulation with a subsequent recovery of the polar vortex after the event. The tropospheric signal of SSWs can persist for up to two months after the occurrence of each event

[Charlton and Polvani, 2007]. This signal is particularly strong and persistent after a subset of SSWs, called Polar-night Jet Oscillation events (PJOs), which are characterized by a very persistent warm polar lower stratosphere [Hitchcock et al., 2013].

The importance of polar vortex variability for both atmospheric dynamics and ozone chemistry has spurred considerable efforts in identifying if and how the stratospheric polar vortex might respond to increasing greenhouse gases (GHGs). While several studies have been devoted to this question, there is not consensus at this time on which projected changes to the polar vortex are robust. Here, and throughout the paper, we use the word robust to mean a strong agreement across many models as to the size and amplitude of the changes to the stratospheric polar vortex under increased GHG. To offer a trivial example: a two-model ensemble in which one model predicted a halving of SSW frequency and the other model predicted a doubling of SSW frequency would not represent a robust prediction of future changes, although both these changes might be statistically significant in each model. On the contrary, if one model predicted a significant increase of SSW frequency by a factor of 2.5 and the other by a factor of 2, we would regard this as a robust prediction.

Early studies using simple models demonstrated polar stratospheric cooling under increased GHG forcing [Manabe and Wetherland, 1967; Fels et al. 1980]. Global atmospheric modeling work in the 1990s (with prescribed changes in sea surface temperatures) projected a boreal polar warming in winter, but no consensus on the changes in the number of SSWs [Rind et al. 1990; Mahfouf et al 1994; Rind et al. 1998; Butchart et al 2000]. Moreover, after decades of improvement in modeling the stratosphere, a clear consensus about future changes to the polar vortex is still missing. For instance, one can find in the literature a number of single-model studies that report a significant increase in the frequency of SSWs in the future [Charlton-Perez et al., 2008; Bell et al., 2010], while other studies report a non-statistically significant increase [e.g. Mitchell et al., 2012a; Ayarzagüena et al. 2013], and others no significant change in SSW frequency at all [McLandress and Shepherd, 2009; Scaife et al., 2012; Karpechko and Manzini, 2012]. Multi-model intercomparisons of Chemistry Climate Model Validation (CCMVal) and Coupled Model Intercomparison Project 5 (CMIP5) models have reported large discrepancies in the sign of change among models [Mitchell et al. 2012b; Kim et al., 2017].

Recently, Ayarzagüena et al. [2018] revisited this topic, trying to overcome some of the issues suggested in the literature as potential reasons for this disagreement, such as the use of one single model in the analysis or the dependence of results on the SSW identification criterion. They analyzed 12 different models participating in the Chemistry Climate Model Initiative (CCMI) and applied several different (absolute and relative) criteria for the identification of SSWs. The outcome was again a lack of a significant change in SSWs frequency in the future, although most of the models predicted a slight increase in the frequency of these, regardless of the SSW identification algorithm. One might argue, however, that the limited data record available (40 years in each period of study), and the relatively moderate GHG forcing used in the central CCMI scenario (Representative Concentration Pathway 6.0, RCP6.0), might be insufficient to detect significant changes in SSWs in those simulations.

The new CMIP6 model generation together with the special data requirements of the DynVarMIP project [Gerber and Manzini, 2016] provide a new opportunity to revisit the question of the effects of increasing CO_2 on the interannual variability of the stratospheric polar vortex. The very long daily data record at stratospheric levels of the Diagnostic, Evaluation and Characterization of Klima (DECK) experiments allows us, for the first time, to try to isolate

forced changes in stratospheric variability in a larger ensemble of high-top models than possible previously [Eyring et al. 2016]. Specifically, one of these DECK simulations consists in a very high CO_2 forcing (abrupt4xCO_2) enabling the exploration of changes in the vortex variability under an extreme future scenario. Furthermore, the daily output of the 1pctCO_2 simulation with a gradual increase of CO_2 allows us to investigate the time of emergence of SSW changes.

The goal of this study is to analyze the potential changes in the interannual variability of the polar vortex due to increasing CO_2 concentrations, as simulated by CMIP6 models. Apart from the mentioned new possibilities opened up by the availability of CMIP6 data, we have also examined other characteristics that are relevant for the stratosphere-troposphere coupling such as the seasonal cycle of the polar vortex, i.e. formation and final breakdown, in both hemispheres, as well as changes in stratosphere-troposphere coupling during SSWs, given the importance of these aspects for tropospheric impacts and predictability. However, we do not aim here to fully diagnose stratospheric variability in the CMIP6 models, nor to explain why models differ in their estimates of the sensitivity of the stratospheric polar vortex to CO_2 forcing. Instead, we simply aim to provide a timely, quantitative estimate of how stratospheric variability might change under CO_2 forcing since this information is of critical importance to the upcoming Intergovernmental Panel on Climate Change (IPCC) AR6 report, and for future work on the stratosphere in CMIP6 models.

2 Data and methodology

2.1 Data

In this study we analyze the daily output of DECK simulations by 12 CMIP6 models participating in the DynVarMIP initiative (Table 1). All the models are coupled to an ocean and sea ice model, and most (8 out of 12) are “high-top” models, defined by having a model top at or above 0.1hPa as in Domeisen et al. [2019]. A priori, we expect the high-top models to have more realistic polar stratospheric variability and, consequently, to better simulate SSWs, and their frequency and surface impacts, than low-top models [Charlton-Pérez et al. 2013]. For the CMIP6 ensemble, there are a much larger number of models that have a high model top than in the previous CMIP5 ensemble. In order to make sure our model sample is unbiased, only a single member of each model ensemble is analyzed here; details are shown in Table 1.

We focus on four DECK experiments [Eyring et al., 2016], each of them used for different purposes. The historical run is employed for model validation: we compare the simulated SSW frequency, intensity and seasonality to the values obtained from the JRA-55 reanalysis [Kobayashi et al., 2015]. In fact, we have specifically restricted the analysis period to 1958-2014 to perform a rigorous quantitative comparison with JRA-55.

The piControl experiment is used for two purposes. Since it contains a very long data record (more than 450 years for most of the models, Table 1), it is used to characterize both the baseline estimates of SSW frequency and intensity, and to characterize internal atmospheric variability in SSW frequency and trends.

174 **Table 1.** List of models included in the analysis indicating their resolution and the ensemble
175 members considered in simulations. Equilibrium climate sensitivity for CO_2 doubling is taken
176 from analysis by A. G. Pendergrass using Gregory et al. [2004] method
177 (https://github.com/apendergrass/cmip6-ecs)

178

Models	Model resolution	Ensemble members	Internally generated QBO	Nr. of years piControl run	Equilibrium Climate Sensitivity / K
CanESM5 [Swart et al. 2019a,b]	T63L49, top 1hPa	r1i1p2f1	No	450	5.59
CESM2 [Danabasoglu et al. 2019a, b]	1ºx1º L32, top 40km	r1i1p1f1	No	1200	5.12
CESM2-WACCM [Danabasoglu, 2019; Gettelman et al. 2019]	1ºx1º L70, top 150km	r1i1p1f1	Yes	500	4.61
CNRM-ESM2-1 [Séférian, 2018; Séférian et al. 2019]	TI127L91, top 0.01hPa	r1i1p1f2	Yes	500	4.66
GFDL-CM4 [Guo et al. 2018; Held et al. 2019]	C96L33, top 1hPa	r1i1p1f1	No	140	3.84
GISS-E2-2-G [NASA-GISS et al. 2018]	2ºx2.5º, top 0.002hPa	r1i1p1f1	Yes	81	
HadGEM3-GC31-LL [Roberts, 2017 Williamson et al. 2018]	N261L85, top 85km	r1i1p1f3 except for piControl run: r1i1p1f1	Yes	500	5.41
INM-CM5-0 [Volodin et al. 2017]	2x1.5L73, top 0.2hPa	r1i1p1f1	Yes	154	2.1
IPSL-CM6A-LR [Boucher et al. 2018]	N96, top 80km	r1i1p1f1	Yes	1200	4.49
MIROC6 [Tatebe et al. 2018; 2019]	T85L81, top 0.004hPa	r1i1p1f1	Yes	800	2.54
MRI-ESM2-0 [Yukimoto et al. 2019a b]	TL159L80, top 0.01hPa	r1i1p1f1	Yes	200	3.30
UKESM1-0-LL [Tang et al., 2019; Kuhlbrodt et al. 2018]	N96L85, top 85 km	r1i1p1f2	Yes	1100	5.27

179

180 The abrupt4xCO_2 and 1pctCO_2 runs are used to examine the impact of CO_2 forcing on
181 SSW properties. Both simulations extend 150 years (except for the abrupt4xCO_2 in IPSL-

CM6A-LR, which is 900 years long, and GISS-E2-2-G, which is 81 years long). All forcings in the abrupt4xCO_2 simulations are identical to those in the piControl run, except for the CO_2 concentrations, which is abruptly quadrupled from piControl levels, and then are held constant throughout the entire length of the simulation [Eyring et al. 2016]. The large and constant forcing in the abrupt4xCO_2 makes it possible to isolate robust changes, if any, to the size and nature of changes to SSW properties. In the 1pctCO_2 simulation, the CO_2 concentration starts at pre-industrial levels and is increased at the rate of 1% per year. This simulation is used to estimate the rate at which SSW frequency might change in the future [one aspect of the so-called 'dynamical sensitivity' of the stratosphere, Grise and Polvani 2016].

Anomalies are defined as the departure from the daily evolving annual cycle of each respective model. In the piControl run, the climatology is based on the whole period, while in the historical run only the 1979-2014. In the abrupt4xCO_2 runs, a trend is identified in some variables during the first 50 years following the switch-on of the forcing. To avoid this trend, the climatologies are computed after omitting the first 75 years except for IPSL-CM6A-LR where we omit the first 300 years as its integration extends longer than 400 years. A similar omission of data is performed for the analysis of SFW or vortex formation dates. In contrast, the full abrupt4xCO_2 is considered when looking at SSW frequency as no trend is detectable in the occurrence of these phenomena.

2.2 Methods

There has recently been a considerable discussion in the literature as to which metrics best characterize the variability of the stratospheric polar vortex, in particular, extreme vortex weakening events [Butler et al. 2015; Butler and Gerber, 2018]. However, in a recent study, Ayarzagüena et al. [2018] found little dependence on the choice of metrics in terms of documenting future changes in SSWs. Thus, we here focus only on a few, widely-used and easily implementing metrics of stratospheric variability. Future work will likely be able to explore stratospheric variability in more detail, and possibly reveal subtleties in changes to stratospheric circulation not apparent in our initial analysis. Furthermore, focusing on commonly used diagnostics allows us to place our work in the context of previously published studies on changes in, for example, SSW frequency.

Several aspects of the stratospheric polar vortex (formation, final breakdown and variability) are analyzed using the zonal mean zonal wind at 60ºN and 10hPa ($u_{60N10hPa}$) for the NH, and 60ºS and 10hPa for the SH.

- SSWs are identified following the criterion proposed in Charlton and Polvani [2007], which is based on the reversal in the sign of $u_{60N10hPa}$ from November to March. Their criterion includes two additional restrictions: (1) winds must return to westerly for at least 20 consecutive days between events and (2) winds must return to westerly for at least 10 consecutive days before April 30 of each year. Recall that this definition only identifies so-called "major" SSWs. Here we do not examine other aspects of polar vortex variability, such as vortex intensification events, wave reflection events, or minor stratospheric warmings.
- SFWs is defined as the last date in the spring on which $u_{60N10hPa}$ reverses and does not return to westerly for more than 10 consecutive days [Butler and Gerber, 2018].
- The polar vortex formation date is identified as the first time that $u_{60N10hPa}$ turns westerly after 1 July, in the NH, and stays westerly for at least 10 days.

- PJOs are identified by applying a slight variation of criteria established by Hitchcock et al. [2013], as the original required finer vertical resolution than available. The new metric has been validated in reanalysis to ensure that similar results are obtained in this case as to those obtained by applying the original one (not shown). Here, the identification is based on two time series PC_1 = T'(5 hPa) - T'(100 hPa) and PC_2 = T' (50 hPa), where T' indicates the polar-cap averaged temperature anomaly (from climatology) at the specified pressure level. These time series are transformed into polar coordinates r(t) and phi(t), and the central dates of events are defined by when the phase phi(t) passes counter-clockwise through $3\pi/2$, so long as the amplitude r(t) is greater than 2.5σ. Once a central date is defined, the starting date of the event is defined by the most recent date prior to the central date when r(t) is below 1.5σ, and similarly the ending date of the event is defined by the earliest date following the central date when the r(t) is below 1.5σ.

2.2 Statistical methods

Two methods to calculate the statistical significance of changes to the SSW frequency are used: a parametric method based on an assumption that the SSW frequency can be estimated using a Poisson point process, and a non-parametric bootstrapping technique based on resampling the piControl run of each model. Trends in SSW frequency and the time of emergence of these trends are estimated by fitting a Generalized Linear Model (GLM) to the decadal SSW frequency estimates from each model. All three statistical methods are described in detail in Appendix 1.

3 Model simulation of SSWs during the Historical Period: Mean frequency and seasonal distribution

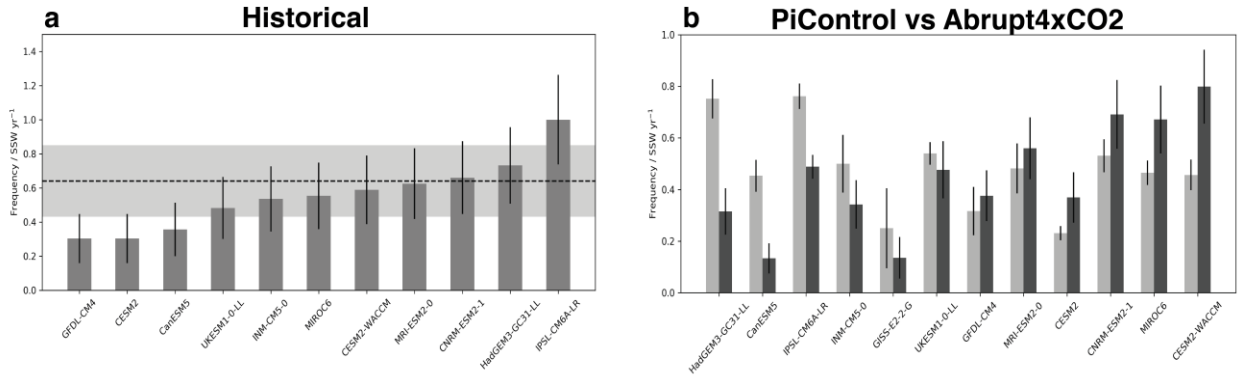

Figure 1. **(a)** Average annual SSW frequency in the historical simulations (1958-2014) of the 11 models. Black lines show 95% confidence estimates for the annual frequency. Dashed black line corresponds to SSW frequency in the JRA-55 reanalysis, with its 95% confidence interval in the light gray shading. **(b)** Same as (a) but for SSW occurrence in the piControl (light gray bars) and abrupt4xCO_2 simulations (dark gray bars). Black lines show 95% confidence intervals for each estimate. Bars are ordered by the size of the difference between the two simulations.

Prior to reporting changes in SSWs caused by increased CO_2 concentrations, it is important to document the models' ability to simulate SSW events during the period of overlap

with re-analysis data: we do so by analyzing the historical simulations. Figure 1a shows the average frequency of SSWs during the period 1958-2014 in JRA-55 reanalysis (horizontal dashed line) and the corresponding value for the CMIP6 models (bars; the numerical values are given in Table S1). In agreement with prior studies [e.g., Charlton-Perez et al. 2013; Ayarzagüena et al. 2018] we find a large spread across the models in the mean frequency of SSW over that period. This spread is likely due, in part, to the large internal variability of the polar wintertime stratosphere; even with an identical climate model the frequency of SSWs can vary greatly across different realizations, as demonstrated by Polvani et al. [2017].

Mindful of this large internal variability, it appears that only four of the models are significantly different from JRA-55, at the 95% confidence level. Three of these are the models with the lowest model tops (CESM2, CanESM5 and GFDL-CM4) that simulate fewer SSW events than JRA-55 re-analysis. When comparing the seasonal distribution of SSW activity in these models with JRA-55 (Fig. 2) it is clear that for two of them (GFDL-CM4 and CESM2), the SSW activity is significantly shifted towards March, with few SSWs observed in December and January. This is another common bias in low-top models [Charlton-Perez et al., 2013], and more generally, in models with an overly strong polar vortex. It is also worth noting that the three low-top models mentioned above are the only ones lacking a simulated Quasi-Biennial Oscillation (QBO). The fourth model with an unrealistic SSW frequency (IPSL-CM6A-LR), in contrast, simulates a very high number of SSWs, on average one per year during the historical period (instead of one every other year). As detailed below, this model also stands out for its high frequency of warmings in the piControl run. While we retain these four models in our analysis, the simulated changes produced by these models should be treated with caution given these biases.

Finally, considering the surprising occurrence of an SSW in the SH in 2002 [Krüger et al. 2005], we extended the analysis to that hemisphere. Not a single SSW event was identified in the SH over the historical period in the models analyzed here. One may be tempted to claim that the CMIP6 models are underestimating the stratospheric variability in the SH, as spontaneous SSWs in the absence of stationary waves have been reported in simple models [Kushner and Polvani, 2005]. However, it remains to be demonstrated whether five or six decades of observations are sufficient to make that claim.

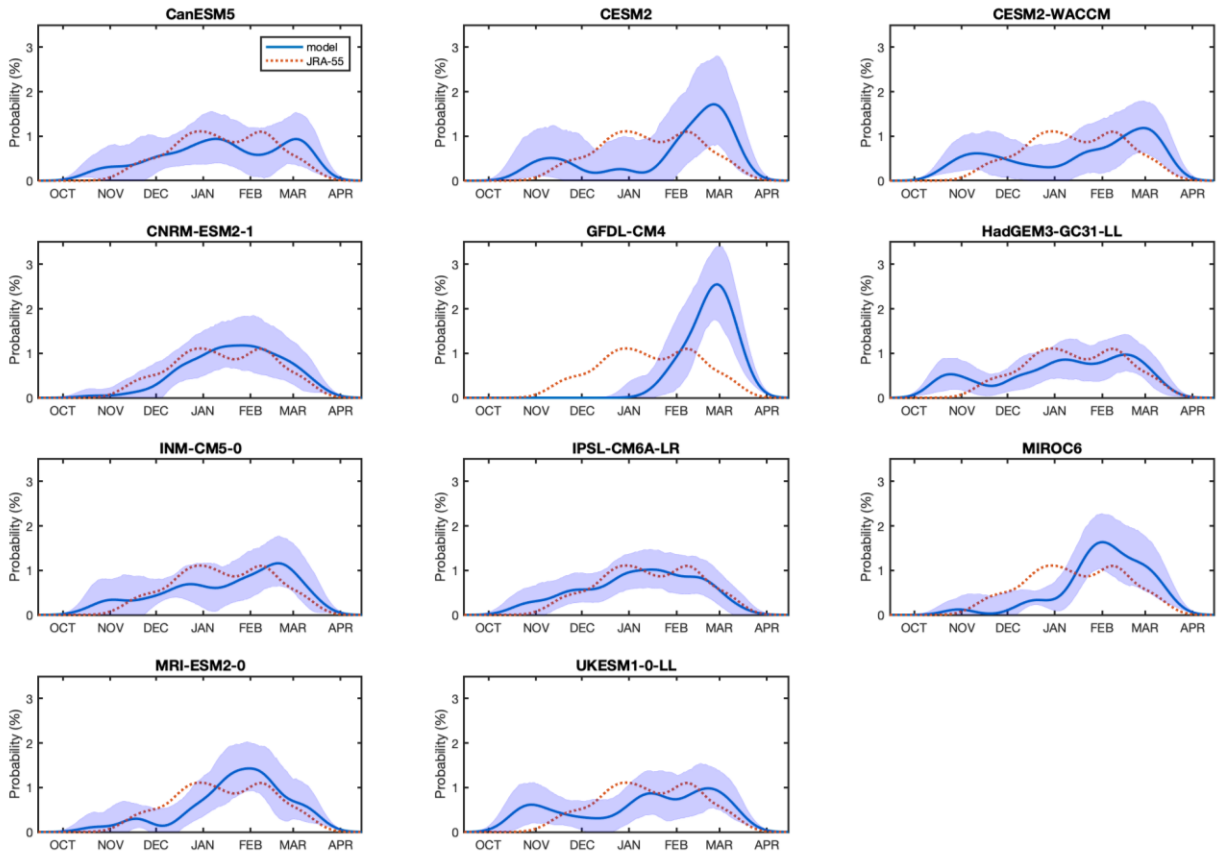

Figure 2. SSW frequency distribution in the historical simulation of each model (blue line) and JRA-55 reanalysis period (orange dashed line). The distribution has smoothed by a kernel smoother of a bandwidth of 10 days. Shading corresponds to 2.5th-97.5th percentile range of the bootstrap samples i.e., the 95% confidence interval on the mean of the piControl simulation. (See more details about the determination of this interval in Appendix).

4 Future changes in polar stratospheric variability

4.1 Future changes in sudden stratospheric warmings

Figure 1b displays the mean frequency of SSWs in both the piControl and abrupt4xCO_2 simulations (numerical values in Table S2). As discussed in Section 2, all SSWs identified in the entire abrupt4xCO_2 simulation have been considered. We stress, however, that the main results presented below do not change significantly if only the last 75 years of each abrupt4xCO2 simulation are used (not shown). Two different tests of the statistical significance of the changes are conducted, providing a consistent indication of the statistical significance of changes, although the precise p-values vary due to difference in the underlying assumptions.

Of the 12 models in our study, four models indicate a statistically significant *decrease* in SSW frequency, while four indicate a statistically significant *increase* in SSW frequency. Thus, no consensus in the sign of the change exists in the CMIP6 models, in agreement with the diversity of claims reported in the earlier literature. The lack of a robust change across the

models is not due to a lack of sensitivity of SSW frequency to increasing CO_2: in fact, 8 of the 12 models indicate significant changes. Rather, the CMIP6 models suggest that there is a great deal of uncertainty in the sign of the change, which varies between a near doubling in the frequency of SSWs in some models, to a near halving in others. These divergent responses of the models may now be clearer in the CMIP6, where we can consider a stronger forcing ($4xCO_2$) and have access to longer records of daily data, compared to previous studies.

We also note that the lack of consensus in the CMIP6 models agrees with the recent study of Ayarzagüena et al. [2018], who analyzed the chemistry climate model projections of the CCMI models, which were forced with RCP6.0 scenario. While reporting a general tendency towards an increased frequency of SSWs by the end of the current century, they also emphasized that most changes were *not* statistically significant.

We do not attempt to further analyze the causes of differences in the model responses here, other than to note that within our set of models, one of the models indicating a significant reduction of SSW frequency (CanESM5) and one of the models indicating a significant increase of SSW frequency (CESM2) have anomalously low SSW frequency and (in the case of CESM2) a biased seasonal distribution of SSW in the historical simulations (Fig. 2). Additionally, the two models which show robust decreases in SSW frequency (HadGEM3-GC31-LL and IPSL-CM6A-LR) have the highest frequency of SSW events in the piControl and historical simulations. The IPSL-CM6A-LR has a significant bias in SSW frequency and presents some strong biases in the representation of QBO in the abrupt$4xCO_2$ simulation.

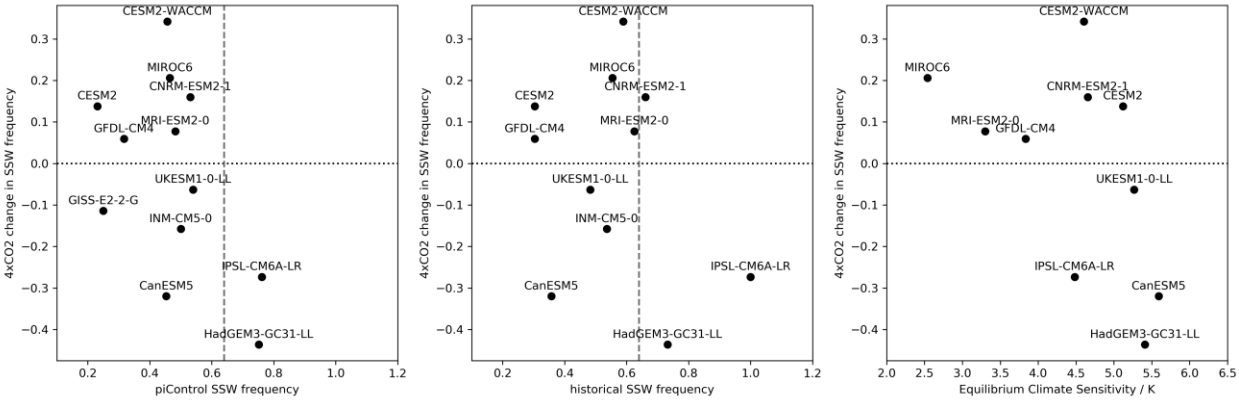

Figure 3: Scatter plots of the change of SSW frequency between the piControl and abrupt$4xCO_2$ simulations vs. the frequency in the piControl simulations, in the historical simulations and the ECS. In the first two plots, the grey dashed line shows the observed SSW frequency in the JRA-55 re-analysis (0.64 SSW yr^{-1}).

We also briefly examined the relationship between the change in SSW frequency and possible predictors of the change, including the frequency of SSWs in the piControl and historical simulations and the Equilibrium Climate Sensitivity (ECS, Gregory et al. [2004]) (Fig. 3). Recall that ECS gives a measure of the equilibrium change of the global surface temperature after a doubling CO_2. As can be seen from Fig. 3, models that have a larger frequency of SSWs in the piControl run and models that have a larger ECS seem to produce large reductions in SSW frequency under large CO_2 forcing. The correlation between SSW frequency changes and ECS is

-0.52 with a p-value of 0.12. The correlation between piControl frequency and SSW frequency changes is -0.50 with a p-value of 0.10. Further analysis of a larger ensemble would be required to determine the robustness of these relationships. Although not addressed in the literature, a relationship between ECS and SSW frequency changes might be possible given some previous results connected to this topic. Shepherd and McLandress, [2011] and Grise and Polvani [2016] documented a link between the strengthening of the sub-tropical jet and stratospheric wave driving. Moreover, Li et al. [2007] have argued that the subtropical jet, and tropospheric state in general, might control the upward planetary wave propagation.

To further examine the changes in SSW frequency under 4xCO_2 forcing, we have analyzed the entire distribution of daily $u_{60N10hPa}$ in December-January-February in the piControl and abrupt4xCO_2 simulations (Fig. 4). The four models with a significant decrease in SSWs frequency in Fig. 1b (HadGEM3-GC31-LL, CanESM5, IPSL-CM6A-LR, INM-CM5-0) are also those that show the largest shift of the $u_{60N10hPa}$ distribution towards stronger vortex speeds in the abrupt4xCO_2 experiment. Interestingly, the opposite does not always apply to models with a significant increase in SSWs. The models with the largest changes in SSW frequency, MIROC6 and CESM2-WACCM show small changes to either the median or standard deviation of the $u_{60N10hPa}$ (Table S3). This would agree with the results of Taguchi [2017] who pointed out SSW frequency does not only correlate with vortex strength but also wave activity.

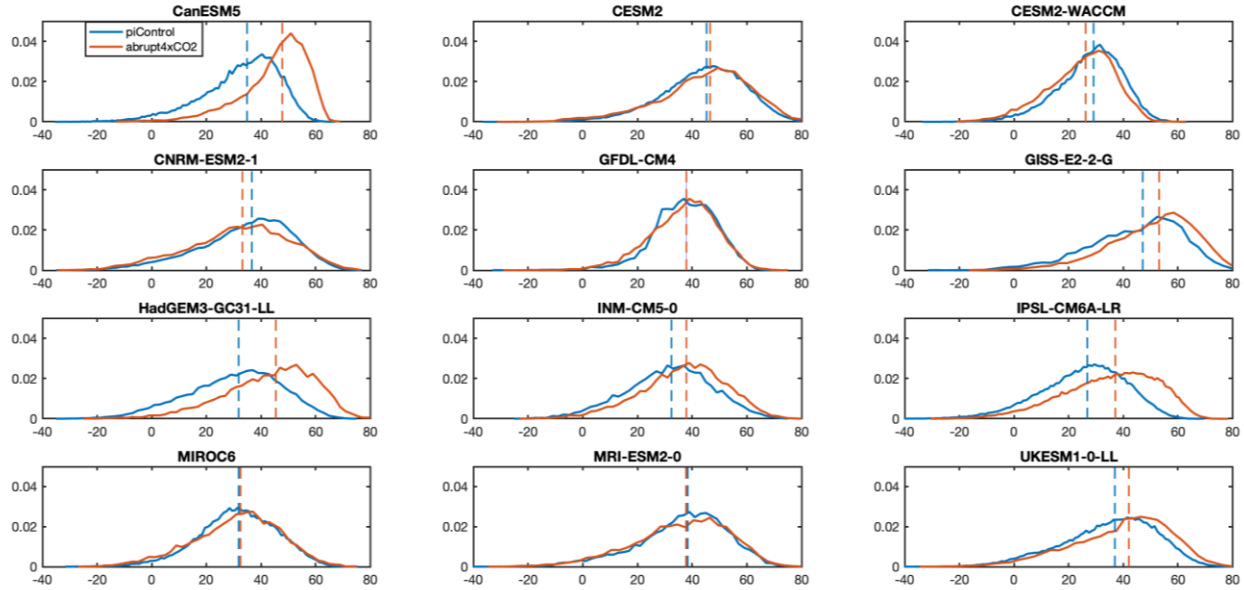

Figure 4. Probability distribution of daily zonal mean zonal wind at 60ºN and 10hPa (m/s) for the piControl (blue) and abrupt4xCO_2 (orange) experiments. Dashed lines represent the median value of the distribution in each integration.

A similar analysis was repeated for the zonal-mean zonal wind at 10hPa averaged between 70º and 80ºN (not shown). That latitude band was found by Manzini et al. [2014] to display significant future changes in wind in most models, unlike the 60ºN latitude where no

robust future changes were found in CMIP5 models because the opposed effects of subtropical jet and stratospheric polar vortex changes might combine at that latitude. However, in our case, the main conclusions remain the same. Those models that show a shift of the $u_{60N10hPa}$ distribution towards stronger vortex speeds under 4xCO2 forcing also display a sharper peak of high values u at 70-80ºN suggesting lower variability in that region, consistent with a stronger and larger vortex.

We have also examined potential changes in SSW seasonality. However, despite the already mentioned changes detected in SSW frequency in some models, the drastic increase in CO_2 concentrations does not appear to substantially affect the seasonal distribution of SSWs (not shown).

Finally, motivated by the recent occurrence of a minor but highly publicized SSW event in the SH in September 2019 [Hendon et al., 2019], together with the occurrence of a major SSW in September 2002, we also examined the CMIP6 models to determine the extent to which the likelihood of similar events might change under the extreme climate forcing in the abrupt4xCO_2 runs. Only one of our twelve models (MRI-ESM2-0) simulates an SSW in both the piControl and the abrupt4xCO_2 simulations. Thus, these runs provide no evidence for the claim of possible trends in the frequency of SSWs in the SH that would be caused by increased CO_2 concentrations.

4.2 Trends in SSW frequency and time of emergence

For the model integrations which show a statistically significant increase or decrease in SSW frequency between the piControl and the abrupt4xCO_2 runs, it is useful to consider when and whether the trend in SSW frequency might be detected in a simulation with continuously increasing CO_2 forcing. A useful way to frame climate trends is in terms of the time of emergence of the signal from the unforced climate noise [Hawkins and Sutton, 2012]. This question is examined by studying the occurrence of SSWs in the 1pctCO_2 runs, an idealized scenario.

Trend estimates for each model are shown in the Fig. 5a (numerical values in Table S4). Results reveal that there are six models (light gray bars) for which the null hypothesis of no trend in SSW frequency can be rejected, but consistent with the results of the previous section, the sign of this trend is not robust across models. While CanESM5 and HadGEM3-GC31-LL show a significant decrease, CNRM-ESM2-1, CESM2-WACCM, GFDL-CM4 and MRI-ESM2-0 show a significant increase. Recall that for the abrupt4xCO_2 runs (Fig. 1b), CNRM-ESM2-1 and CESM2-WACCM also indicated a statistically significant increase in SSW frequency compared to the piControl runs, while GFDL-CM4 and MRI-ESM2-0 did not (although they did indicate an increased frequency). CanESM5 and HadGEM3-GC31-LL both showed a statistically significant decrease.

One can also estimate a time of emergence of the trend by comparing the trend in the 1pctCO2 runs with the natural variability in SSW frequency from the piControl run (see Appendix for details in the procedure). For the models with a significant trend, the decade of emergence is shown in Fig. 5b. There is a wide spread in the projected time of emergence for the models with a significant trend, varying from the 5th decade to 14th decade. This result reflects both the variation in the trend across the models and the spread in the estimated variability in SSW frequency (the noise) in the piControl simulations. Since the time of CO_2 doubling occurs

between the 6th and 7th decade in the 1pctCO_2 run and approximately by 2060-70 in the RCP8.5 scenario [Meinshausen et al., 2017], these results indicate that the emergence of a detectable change in SSW frequency is extremely unlikely prior to the end of the 21st century.

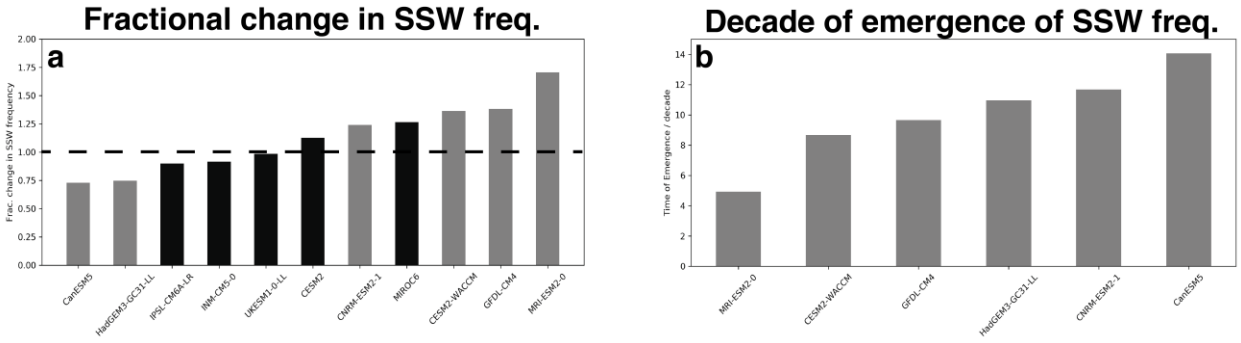

Figure 5. (a) Estimated fractional change in SSW frequency by the seventh decade of the 1pctCO_2 simulations. Light gray shaded lines indicate that the trend of SSW frequency in the model is significantly different from zero at a p-value of 0.05. Dashed line indicates trend equal to 1, i.e. no trend in the SSWs frequency. **(b)** Decade of emergence of SSW frequency trend for those models in which the trend term is significantly different from zero, calculated as described in the main text.

5 Future changes in the seasonal cycle of the polar stratosphere

Since, according to linear theory, the vertical propagation of stationary Rossby waves is restricted to periods with westerly winds, stratospheric variability is largely confined to the winter season [e.g., Charney and Drazin 1961]. When considering how stratospheric variability might change in future climates it is therefore also important to consider the extent to which the timing and length of the winter season in the stratosphere might also change.

Figure 6a and b show the distribution of dates of formation and final breakdown of the boreal stratospheric polar vortex, respectively, in the piControl, historical and abrupt4xCO_2 CMIP6 simulations. In these plots the first years of the abrupt4xCO_2 simulations (75 or 300 years) have been omitted similarly to the procedure followed to calculate the climatology. Nevertheless, conclusions do not change when considering the whole data record for abrupt4xCO_2 runs.

First, let us consider the historical model simulations, and contrast them to the reanalysis. Over the period 1958-2014, the polar vortex forms earlier in all models than it does in the reanalysis, with the exception of IPSL-CM6A-LR. In contrast, the SFW date is well reproduced by models. The later implies an improvement with respect to previous generations of climate models, such as those contributing to CCMVal and CMIP5, which simulated a delayed SFW [Butchart et al., 2011; Kelleher et al., 2019]. CMIP6 models are also good at simulating the different range of interannual variability in the dates of vortex formation and SFW, the latter being considerably larger than the former.

Second, we consider the changes caused by increased CO_2, both for the formation and the final breakdown of the boreal polar vortex: these display robust changes across models. The polar vortex forms earlier and persists for longer in the abrupt4xCO_2 scenario than in the piControl runs (Fig. 6a and b). This signal is particularly clear, and is significant in all models in the case of the vortex formation. Although half of the models do not show a significant change, there is a clear consensus in the sign of the SFW change across these models.

Interestingly, the models with the largest delay of SFW in the abrupt4xCO_2 simulation (CanESM5, HadGEM3.GC31-LL and IPSL-CM6A-LR) are also those with the largest reduction in the frequency of SSWS. This indicates that the long persistence of the vortex is related to a stronger and colder vortex during the extended winter, rather than to the effect of SSWs on the SFWs timing suggested by Hu et al. [2014]. We hypothesize that the year-round radiative effect of CO_2, which is associated with a warming tropical upper troposphere and a cooling stratosphere, increases the upper-level meridional temperature gradient and leads to a longer-lived polar vortex. Why this influence occurs primarily in early fall and spring may be tied to the seasonality of the upper tropospheric warming [Harvey et al. 2013], and the dynamical driving of the polar vortex. Indeed, the wave activity is typically weaker during the transition season (particularly in Autumn) than in mid-winter [Kodera et al., 2003], explaining the dominance of the radiative effect of increased CO_2 on the stratosphere in the former metric. In sum, models predict an increase of around 30 days of westerly winds in the abrupt4xCO_2 simulations, a substantial increase in the time of the year over which stratospheric variability is active and can couple with the troposphere.

A similar analysis has been performed for the SH. Because planetary wave activity is much weaker in the SH than in the NH [Andrews et al. 1987], radiative CO_2 forcing dominates the SH polar vortex response to increasing CO_2 concentrations and so, causes a robust strengthening. In many models the extreme CO_2 concentrations prevent the polar vortex from disappearing at all during austral summer, leading to perpetual westerly conditions in the stratosphere, so we do not show the results for the abrupt4xCO_2 simulation. The distribution of SFW dates for piControl and historical simulations are displayed in Figure 6c. Unlike in the NH, the distribution of SFWs in the SH already shifts towards a later date in the historical period with respect to the piControl conditions. Although the attribution of changes in the length of the winter season to CO_2 is complicated, ozone depletion in austral spring over the historical period might be responsible, based on previous literature [e.g. McLandress et al. 2010; Oberländer-Hayn et al. 2015].

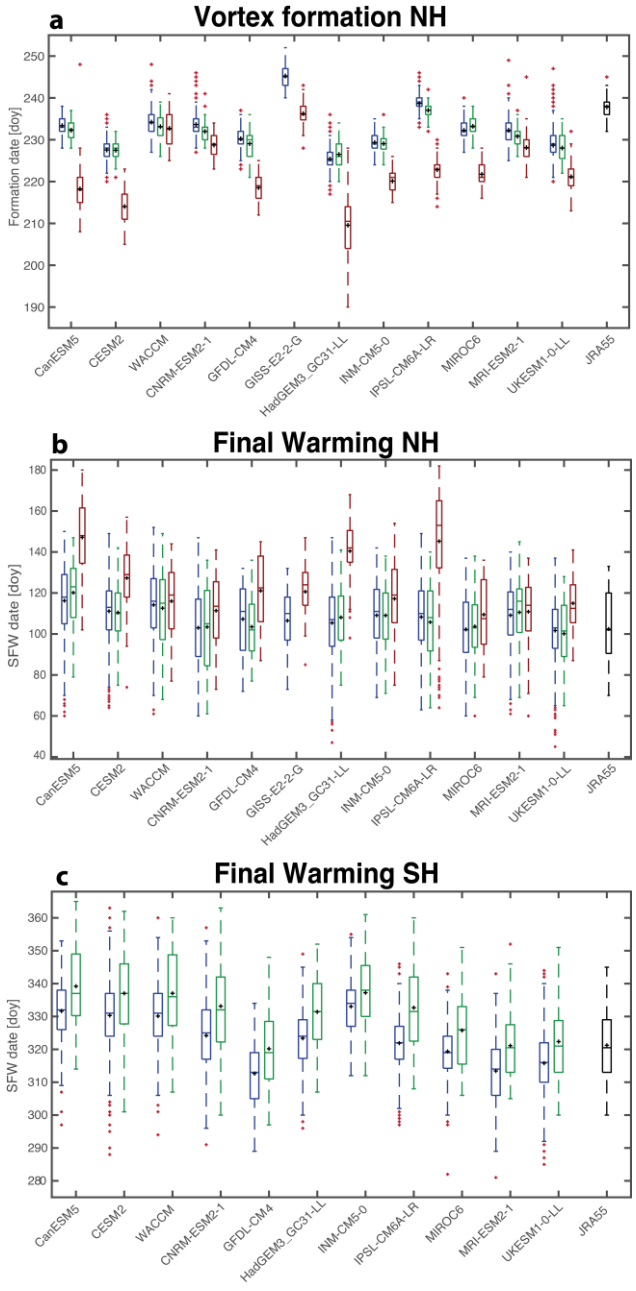

Figure 6. Box plots showing the distribution of dates of **(a)** polar vortex formation and **(b)** stratospheric final warming in the Northern Hemisphere for the piControl (blue), historical (green) and abrupt-4xCO_2 (red) simulations for all models and JRA-55 reanalysis. **(c)** Same as (b) but for the Southern Hemisphere and only in piControl and historical runs. The interquartile range is represented by the size of the box and the inside line (black cross) corresponds to the median (mean). Whiskers indicate the maximum and minimum points in the distribution that are not outliers. Outliers (red crosses) are defined as points with values greater than 3/2 times the interquartile range from the ends of the box.

6 Future changes in the surface impact of SSW events

6.1 Surface response to SSW events

In addition to changes in SSW frequency, amplitude and seasonality, it is also conceivable that the surface impact of SSW events might change as a consequence of increased CO_2. While detailed quantitative description of the mechanism for coupling between SSW events and surface remains elusive, there is now a large body of evidence quantifying the amplitude and spatial structure of the surface pressure and temperature responses following SSW events [e.g., Baldwin and Dunkerton, 2001; Polvani et al. 2017; Butler et al. 2017]. A number of studies point to the importance of eddy-jet feedbacks in determining this surface response [e.g.: Kushner and Polvani, 2004; Song and Robinson, 2004; Garfinkel et al. 2013;]. It is therefore plausible that together with changes in the position and variability of the extra-tropical jet caused by CO_2 increases, one might be able to detect changes in the surface response following SSW events.

To test this idea, we analyze first composite maps of anomalous surface temperature and sea-level pressure (SLP) for the period 15-60 days after SSWs in the piControl simulation (Fig. 7). In nearly all models we obtain the typical SLP and surface temperature patterns following SSWs that are also detected in reanalysis (although CO_2 forcing is different), i.e., negative Northern Annular Mode pattern (particularly over the pole), and Eurasian cooling and Northeastern American warming. None of the models produce a positive SLP anomaly that can be found in the JRA55 composite though. Despite the relatively structural similarities across models, the amplitude of the response can vary by a factor of two or three between them. The amplitudes in five of the eleven models (CESM2-WACCM, GFDL-CM4, HADGEM3-GC31-LL, IPSL-CM6A-LR, and MIROC6) are too weak. The amplitude does not correlate with the SSW frequency. The large SSW sample size from the piControl simulations means that the estimates of surface impact are very robust.

Secondly, we compare the SLP pattern after SSWs in the abrupt4xCO2 and piControl simulations (Fig. 8, differences in SLP between both runs are shown in shading). The overall SSW signal in SLP appears unchanged between the piControl and abrupt4xCO2 simulations, except in three models (CESM2, HadGEM3-GC31-LL IPSL-CM6A-LR) that produce a significantly stronger Northern Annular Mode-like response. However, in the Pacific basin there are some indications about a potential more general change due to a higher CO_2 loading. Indeed, six of the ten models exhibit a statistically stronger negative SLP anomaly in that area under abrupt4xCO_2 forcing than in the piControl runs.

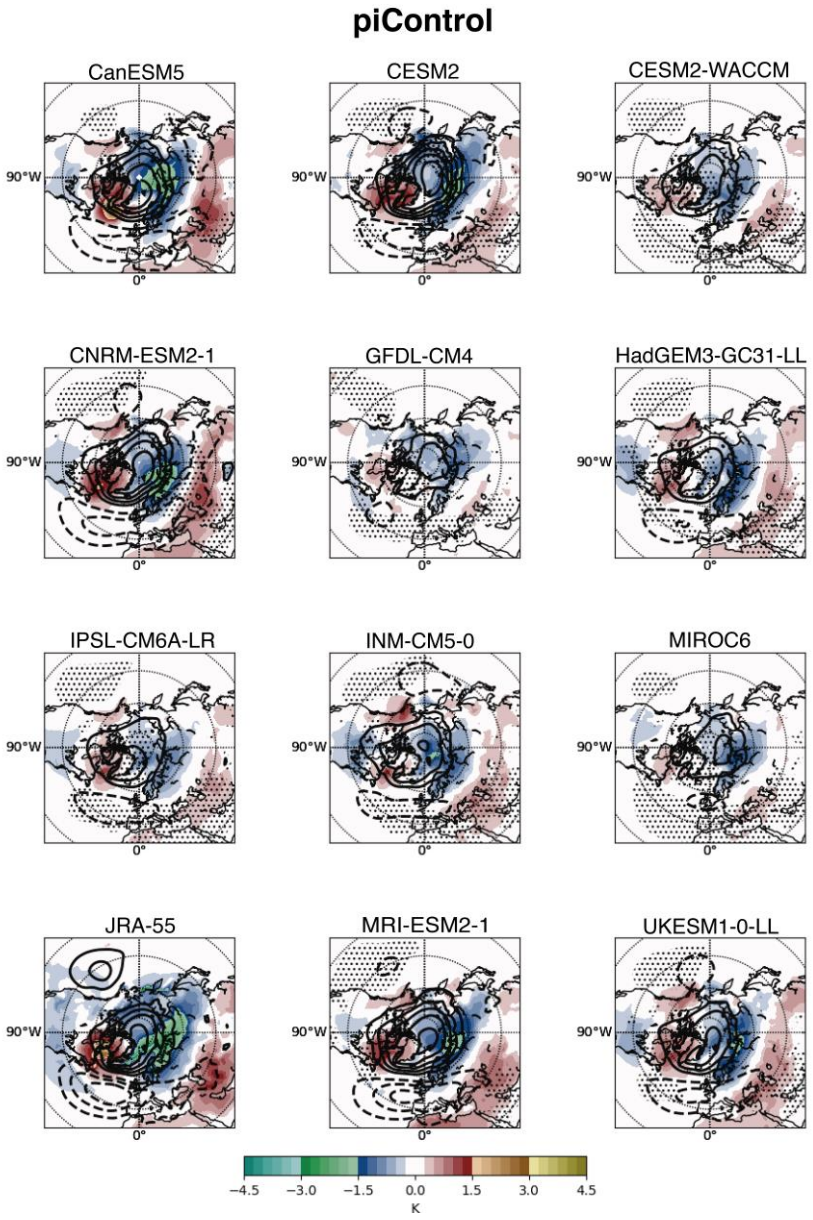

521

522 **Figure 7.** Composite maps of anomalous SLP (contour interval 1hPa) and 2m temperature
523 (shading) for 15/60 days after SSWs in piControl simulation and JRA-55 reanalysis (bottom
524 left). Stippling indicates stat. significant differences in SLP from JRA-55 reanalysis at the 95%
525 confidence level.

526

527

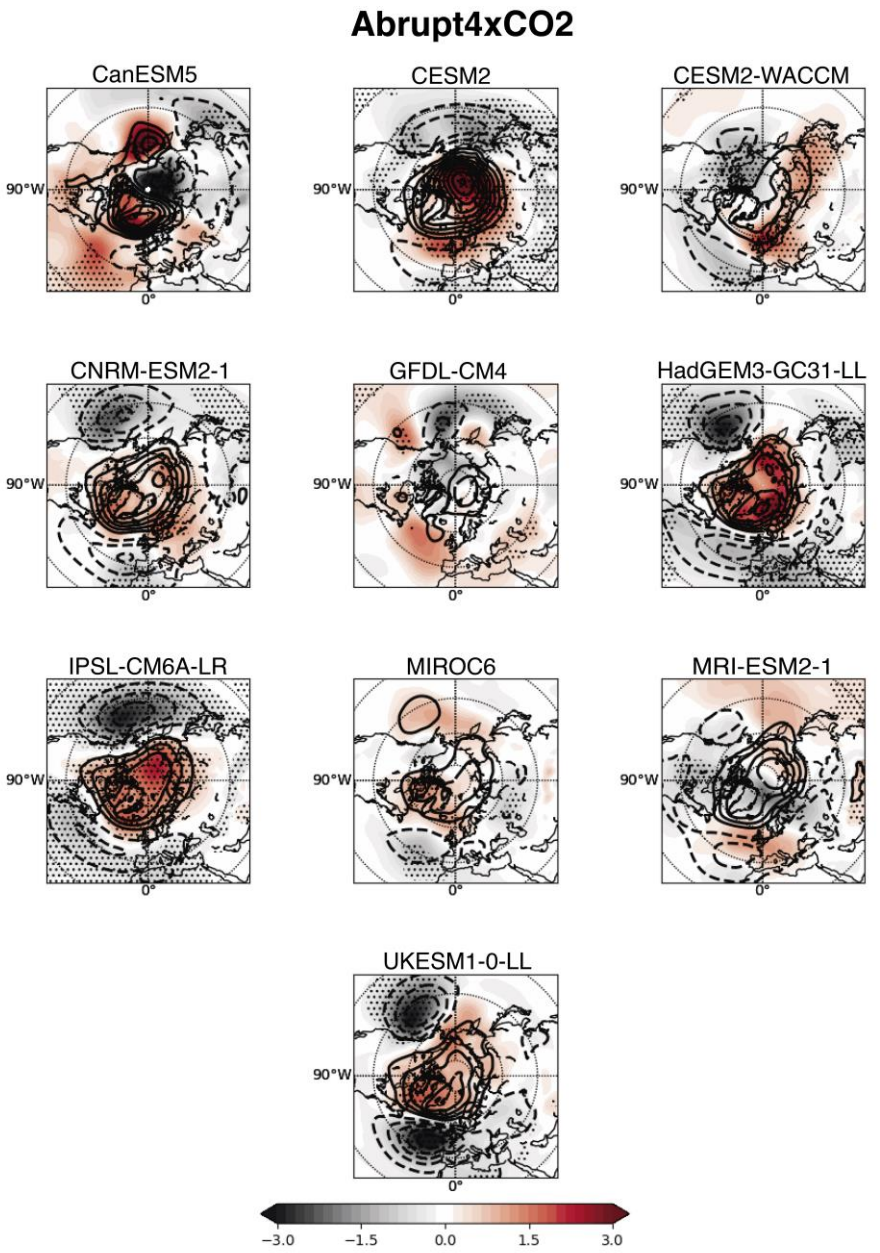

528

529 **Figure 8**. Abrupt4xCO_2-minus-piControl composite maps of anomalous SLP (shading, hPa) for
530 15/60 days after SSWs. Anomalous SLP after SSWs in the abrupt4xCO_2 run is shown in
531 contours (interval: 1hPa). Stippling indicates stat. significant differences from piControl run at
532 the 95% confidence level.

533

534 6.2 Polar-night Jet Oscillation events

535 In this subsection we focus on specific events (PJO events) that are closely related to
536 SSWs and to the stratosphere-troposphere coupling [Hitchcock et al. 2013]. As indicated in the

Introduction section, their strong and persistent tropospheric response explains the interest in investigating possible changes in the occurrence of these events for increasing CO_2 concentrations.

First, examining the surface response to PJOs in the piControl experiment (Fig. S1) confirms that these events in models have a stronger signal in the troposphere than all SSWs too. In JRA-55 roughly half of all SSWs are associated with a PJO event (PJO SSW) (solid bars in Fig. 9). Five models include the JRA-55 value of the ratio of PJO SSW events in their confidence interval in the piControl simulations (MRI-ESM2-0, UKESM1-0-LL, CanESM5, HadGEM3-GC31-LL and GFDL-CM4). The other models underestimate this fraction. However, we do not find a clear relationship between this fraction and the amplitude of SLP pattern following SSWs. For instance, HadGEM3-GC31-LL and GFDL-CM4 simulate a very weak SLP pattern, but the ratio of PJO SSWs is close to observations or even larger (Fig. 7).

In the future, similarly to changes in SSW frequency, there is no robust response of PJO SSWs across models to increasing CO_2 (Fig. 9). Roughly half of the models show a decrease and half of them an increase in PJO SSW events between the piControl and abrupt4xCO2 simulations. More interestingly, two of the three models with a stronger Northern Annular Mode-response to SSWs in the abrupt4xCO_2 run (IPSL-CM6A-LR and HadGEM3-GC31-LL) display an increase in this subset of SSWs too. The other one (CESM2) shows a significant decrease in the fraction of SSWs that are PJOs. Nevertheless, given the low number of models, it is difficult to make a direct link between changes in the number of PJO SSWs and stronger SSW coupling to the surface under increased CO_2 loading.

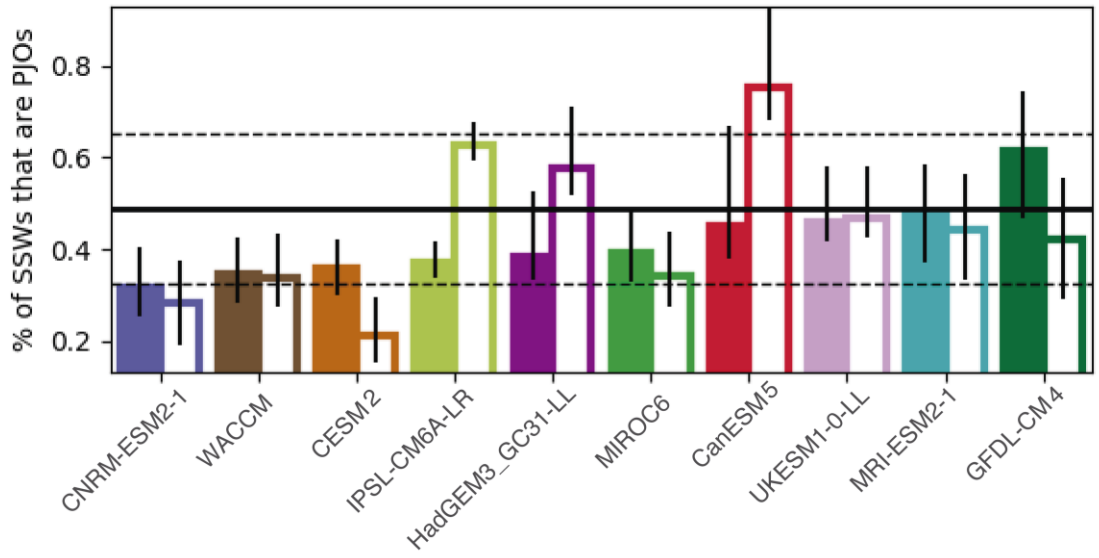

Figure 9. Fraction (%) of SSWs that are also PJO events in piControl (solid bars) and abrupt4xCO_2 (open bar) runs. Horizontal black solid and dashed line correspond to the mean value and the 2.5^{th}-97.5^{th} percentile range in JRA-55 reanalysis, respectively. Error bars are based on bootstrapping

7 Conclusions

SSWs are the primary dynamical event in the wintertime polar stratosphere and have clear impacts on the tropospheric circulation on sub-seasonal to seasonal timescales. This study takes advantage of the new sets of simulations available through the DynVarMIP sub-project of CMIP6 to revisit a number of questions about how SSW events and the stratospheric seasonal cycle might respond to quadrupled CO_2 concentrations. In comparison with previous rounds of CMIP and comparisons made as part of the CCMVal and CCMI projects, the new simulations provide significant advances in our ability to study SSWs. In particular, the long piControl runs and the availability of daily data of abrupt4xCO_2 simulations from a large number of high-top models is unprecedented.

From our analysis of the twelve models for which sufficient daily time resolution stratospheric data was available, these conclusions can be drawn about the impact of extreme CO_2 concentrations on SSW events:

- There is no consensus among models on the sign of changes in SSW frequency.
- It is, however, possible to say with confidence that many models predict that SSW frequency is sensitive to increase in CO_2 forcing.
- There is no change to the impact of SSW events in the N. Atlantic between the abrupt4xCO_2 and piControl simulations. In the N. Pacific, there is some indication that under large CO_2 forcing there will be a larger mean response to SSW events.
- With the exception of MRI-ESM-2-0, predicted trends in SSW frequency are small relative to natural variability (as characterized by the piControl simulations of each model). This is not to say that SSW changes are themselves small (three models predict frequency changes of more than a factor of two compared to piControl conditions) but more a reflection of the large, natural decadal variability in SSW occurrence. As such, changes in SSW frequency are unlikely to be observed until the end of the 21st century.
- Robust changes to the seasonal cycle in the stratosphere are predicted by all models. The stratospheric polar vortex is likely to form earlier and be destroyed later in the future. This extends the season in which the stratosphere can actively couple to the troposphere and influence surface weather.
- There is no evidence of an increased likelihood of major SSWs in the SH in the future.

These results underscore the conclusions of a number of previous studies of SSW events and also motivate the need for more detailed understanding of the stratospheric momentum budget in models as advocated by, for example, Wu et al. [2019], which is now possible with the simulations available through DynVarMIP. Similarly, developing an understanding of how both model formulation and resolution and ECS might influence dynamical sensitivity in the stratosphere remains an important but unsolved challenge for the stratospheric dynamics community.

Acknowledgments, Samples, and Data

BA was supported by the Spanish Ministry of Science, Innovation and Universities through the JeDiS (RTI2018-096402-B-I00) project. The work of LMP is funded, in part, by a grant from the US National Science Foundation to Columbia University. NB was supported by

the Met Office Hadley Centre Climate Programme funded by BEIS and Defra. EPG acknowledges support from the NSF through award AGS-1852727. EM acknowledges support from the Blue-Action project, grant agreement No 727852, European Union's Horizon 2020 research and innovation programme. CO thanks the support and resources provided by the NASA Modeling, Analysis and Prediction program and the NASA High-End Computing (HEC) Program through the NASA Center for Climate Simulation (NCCS) at Goddard Space Flight Center. SW was supported by the "Integrated Research Program for Advancing Climate Models (TOUGOU Program)" from the Ministry of Education, Culture, Sports, Science, and Technology (MEXT), Japan.

We acknowledge the World Climate Research Programme, which, through its Working Group on Coupled Modelling, coordinated and promoted CMIP6. We thank the climate modeling groups for producing and making available their model output, the Earth System Grid Federation (ESGF) for archiving the data and providing access, and the multiple funding agencies who support CMIP6 and ESGF. The authors thank the WCRP SPARC for support of the DynVar Activity, which spurred the formation of the DynVarMIP. CMIP6 data is allocated at the ESGF archive on the following website: https://esgf-node.llnl.gov/projects/cmip6/. The Japanese 55-year Reanalysis (JRA-55) project was carried out by the Japan Meteorological Agency (JMA). JRA-55 data were accessed through NCAR- UCAR Research Data Archive (https://rda.ucar.edu).

Appendix 1: Statistical framework

Statistical methodology for comparing SSW frequency

Parametric method

To compare the frequency of SSW events in two models or between a model and observations, it can be assumed that each data sample is a Poisson process with an annual rate λ_i. The difference between the intensity of the two processes Δ_λ is given in equation (1)

$$\Delta_\lambda = \frac{(\lambda_0 - \lambda_1)}{\sqrt{\frac{\lambda_0}{N_0} + \frac{\lambda_1}{N_1}}} \qquad (1)$$

This can be modeled with a normal distribution providing the frequency of observed events is greater than 30 [Charlton et al. 2007]. This approach has been widely used in the literature.

An alternative approach that compares the ratio of the rate of the two Poisson processes has been studied by Gu et al. [2008].

$$H_0: \lambda_0/\lambda_1 = 1 \qquad against \qquad H_A: \lambda_0/\lambda_1 \neq 1 \qquad (2)$$

Gu et al. [2008] suggest that a conservative test statistic with high power is the one suggested by Huffman [1984] (here X_i is the number of SSWs in each dataset and $\rho = t_0/t_1$ the ratio of the length of observation of the two processes):

$$W(X_0, X_1) = \frac{2[\sqrt{X_0 + 3/8} - \sqrt{\rho(X_1 + 3/8)}]}{\sqrt{1+\rho}} \qquad (3)$$

The p-value for this statistic is estimated as in equation (4), where ϕ is the cumulative distribution function of the standard normal and the observed value of the test statistic $W(X_0, X_1) = w(x_0, x_1)$:

$$p = 1 - 2 * \Phi(w_j(x_0, x_1)) \qquad (4)$$

This is the parametric test statistic used to compare SSW frequency. In addition to calculating the p-value of any test statistic it is also useful, a priori, to estimate the statistical power of any testing framework. Tests with high statistical power minimize the likelihood of Type-II errors (i.e. that the null hypothesis is not rejected when it is, indeed, false). For the test statistic described above, we estimated the statistical power for a comparison with observations of 60 winters with an SSW frequency of 0.6. Assuming a p-value of 0.05, the statistical power of the test is high (above 0.8) for model integrations of more than 100 winters (the null hypothesis will be rejected with a probability above 0.8) which is the case for all comparisons in this study apart from the comparison between the historical simulations and the JRA-55 re-analysis. In this later case, the power of the test is low only for cases in which the observed and modelled SSW frequency is very similar (i.e. for model SSW frequencies of 0.2 and 1 SSW per year, the power is greater than 0.8).

Bootstrapping method

As an alternative to the parametric test, we can also construct a bootstrapping test as outlined by Boos [2003]. We assume that there are two sets of independent samples of the number of SSW events in each season $\{X_1,\ldots,X_m\}$ and $\{Y_1,\ldots,Y_n\}$. To determine the confidence interval for the difference of mean frequency of the two sets $\mu_x - \mu_y$ two samples (of equal size to the original samples) are drawn from the pooled observation set $\{X_1,\ldots,X_m, Y_1,\ldots,Y_n\}$, with replacement. The p-value of the true observation is calculated as the number of bootstrap samples with an absolute difference greater than the true value. In all cases, 10,000 boostrap sample are drawn.

This bootstrapping technique was also applied to determine the confidence intervals on the seasonal distribution of SSW frequency. We choose to perform the bootstrapping on individual winters over a block bootstrapping approach to increase the sample size available for models that have a limited length of piControl simulation available. We have, therefore, assumed that there is no autocorrelation from one winter to the next, but comparison with a block-bootstrapping approach for the models that have long piControl simulations produced similar uncertainty ranges (not shown), indicating that this assumption is reasonable. For Figure 2, the uncertainty range is derived from the piControl simulation. Since there are 57 years in the JRA55 record, we resample 57 years from the piControl simulation, with replacement and recalculate the SSW distribution, normalized by the number of SSWs in that sample. This is repeated 1000 times and the uncertainty range shows the 2.5th to 97.5th percentile range of these 1000 samples (95% confidence interval) i.e., this is the uncertainty range from the model with an equivalent number of years to that of the observations.

Trend in SSW frequency and Time of Emergence

Analogously to the method of Hawkins and Sutton [2012] the time of emergence of a 'signal' in the frequency of SSW events is estimated by comparing the size of the trend in SSW frequency in the 1pctCO2 simulations with the 'noise' determined from the piControl simulation of the same model.

To calculate the signal term in each integration, a Generalized Linear Model fit to the data with a logarithmic link function, implemented in R is used. Trend estimates for decadal SSW frequency in the 1pctCO2 simulations. Modification to the method following (https://stats.idre.ucla.edu/r/dae/poisson-regression/) to account for cases with mild violation of the Poisson distribution in the models is included. The resulting regression equation is of the form:

$$F_{ssw}(t) = e^{\beta_0 + \beta_t t} \qquad (5)$$

Trend terms are expressed as a fractional multiplier of the count per decade. Due to the low mean annual frequency of SSW events, the noise on annual mean frequency estimates is large, therefore when estimating trends in SSW frequency and time of emergence we consider the decadal mean SSW frequency. This means that time of emergence calculations are limited to the decade of emergence.

References

Andrews, D. G., J. R. Holton, and C. B. Leovy, (1987) Middle Atmosphere Dynamics, Academic, Orlando, Fla.

Ayarzagüena B. and E. Serrano (2009) Monthly characterization of the tropospheric circulation over the Euro-Atlantic area in relation with the timing of stratospheric final warmings, J.Clim. 22, 6313-6324.

Ayarzagüena, B., Langematz, U., Meul, S., Oberländer, S., Abalichin, J., and Kubin, A. (2013) The role of climate change and ozone recovery for the future timing of major stratospheric warmings, Geophys. Res. Lett., 40, 2460–2465.

Ayarzagüena, B., Polvani, L.M., Langematz, U., Akiyoshi, H., Bekki, S., Butchart, N., Dameris, M., Deushi, M., Hardiman, S.C., Jöckel, P. and Klekociuk, A., (2018) No robust evidence of future changes in major stratospheric sudden warmings: a multi-model assessment from CCMI. Atmospheric Chemistry and Physics, 18(15), 11277-11287.

Baldwin, M. P and T. J. Dunkerton (2001) Stratospheric harbingers of anomalous weather regimes, Science, 294, 581-584.

Bell, C. J., Gray, L. J., and Kettleborough, J. (2010) Changes in Northern Hemisphere stratospheric variability under increased CO2 concentrations, Q. J. Roy. Meteor. Soc., 136, 1181–1190.

Black, R. X., B. A. McDaniel, and W. A. Robinson (2006) Stratosphere-troposphere coupling during spring onset, J. Clim. 19, 4891-49001.

Black, R. X., and B. A. McDaniel (2007) Interannual variability in the Southern Hemisphere circulation organized by stratospheric final warming events, J. Atmos. Sci. 64, 2968-2974.

Boos D. D. (2003) Introduction to the Boostrap World. Statistical Science, 18 (2), 168-174.

723 Boucher, O., S. Denvil, A. Caubel, M.A. Foujols (2018). IPSL IPSL-CM6A-LR model output
724 prepared for CMIP6 CMIP. Version 20190722.Earth System Grid Federation.
725 https://doi.org/10.22033/ESGF/CMIP6.1534

726 Butchart, N., J. Austin, J. R. Knight, A. A. Scaife, and M. L. Gallani (2000) The response of the
727 stratospheric climate to projected changes in the concentration of well-mixed greenhouse
728 gases from 1992 to 2051, J Clim, 13, 2141-2159.

729 Butchart, N., and Coauthors (2011) Multimodel climate and variability of the stratosphere. *J.*
730 *Geophys. Res.*, 116 (D5), doi:10.1029/2010jd014995.

731 Butler, A.H., J. Sjoberg, D. Seidel., and K.H. Rosenlof (2017) A sudden stratospheric warming
732 compendium, Earth Syst. Sci. Data, 9, 63-76.

733 Butler, A. H., and E. P. Gerber (2018), Optimizing the definition of a sudden stratospheric
734 warming, J. Clim., 31, 2337-2344, doi: 10.1175/JCLI-D-17-0648.1

735 Charlton, A. J., and L. M. Polvani (2007), A new look at stratospheric sudden warmings. Part I:
736 Climatology and modeling benchmarks, J. Clim., 20, 449–469.

737 Charlton, A. J, L. M. Polvani, J. Perlwitz, F. Sassi, E. Manzini, K. Shibata, S. Pawson, J. E.
738 Nielsen, and D. Rind (2007), A New Look at Stratospheric Sudden Warmings. Part II:
739 Evaluation of Numerical Model Simulations, J. Clim., 20, 470–88.

740 Charlton-Pérez, A. J., L. M. Polvani, J. Austin, and F. Li (2008) The frequency and dynamics of
741 stratospheric sudden warmings in the 21st century, J. Geophys. Res. 113, D16116, doi:
742 10.1029/2007JD009571.

743 Charlton-Pérez, A. J. and coauthors (2013) On the lack of stratospheric dynamical variability in
744 low-top versions of the CMIP5 models, J. Geophys. Res. Atmos., 118, 2494–2505,
745 doi:10.1002/jgrd.50125.

746 Charney, J. G., and P. G. Drazin (1961), Propagation of planetary-scale disturbances from the
747 lower into the upper atmosphere, J. Geophys. Res., 66, 83–109,
748 doi:10.1029/JZ066i001p00083.

749 Danabasoglu, Gokhan (2019). NCAR CESM2-WACCM model output prepared for CMIP6
750 CMIP. Version 20190730. Earth System Grid Federation.
751 https://doi.org/10.22033/ESGF/CMIP6.10024

752 Danabasoglu, G., D. Lawrence, K. Lindsay, W. Lipscomb, G. Strand (2019a). NCAR CESM2
753 model output prepared for CMIP6 CMIP historical. Version 20190730.Earth System Grid
754 Federation. https://doi.org/10.22033/ESGF/CMIP6.7627.

755 Danabasoglu, G. and coauthors (2019b) The Community Earth System Model version 2
756 (CESM2), Journal of Advances in Modeling Earth Systems, under review.

757 Domeisen D.I.V, and coauthors (2019): The role of the stratosphere in subseasonal to seasonal
758 prediction. Part I: Predictability of the stratosphere, Journal of Geophysical Research:
759 Atmospheres, https://doi.org/10.1029/2019JD030920.

760 Eyring, V., Bony, S., G. A. Meehl, C. A. Senior, B. Stevens, R. J. Stouffer, and K. E. Taylor
761 (2016), Overview of the Coupled Model Intercomparison Project Phase 6 (CMIP6)

762 experimental design and organization, Geosci. Model Dev., 9, 1937-1958,
763 doi:10.5194/gmd-9-1937-2016.

764 Fels, S. B., J. D. Mahlman, M. D. Schwarzkopf and R. W. Sinclair (1980) Stratospheric
765 sensitivity to perturbations in ozone and carbon dioxide: radiative and dynamical
766 response, J. Atmos. Sci, 37, 2265-2297.

767 Garfinkel, C. I., D. W. Waugh, and E. P. Gerber (2013) The effect of tropospheric jet latitude on
768 coupling between the stratospheric polar vortex and the troposphere, J. Atmos. Sci., 26,
769 2077-2095.

770 Gerber, E. and E. Manzini (2016) The dynamics and variability model intercomparison project
771 (DynVarMIP) for CMIP6: assessing the stratosphere-troposphere system, Geosci. Model
772 Dev., 9, 3413-3425.

773 Gettelman, A. and coauthors (2019) The Whole Atmosphere Community Climate Model Version
774 6 (WACCM6), Journal of Geophysical Research: Atmosphere,
775 https://doi.org/10.1029/2019JD030943

776 Gregory J. M., W. J. Ingram, M. A. Palmer, G. S. Jones, P. A. Stott, R. B. Thorpe, J. A. Lowe, T.
777 C. Johns and K. D. Williams (2004) A new method for diagnosing radiative forcing and
778 climate sensitivity. Geophys. Res. Lett., 31, L03205, doi: 10.1029/2003GL018747.

779 Grise, K.M. and Polvani, L.M., (2017). Understanding the time scales of the tropospheric
780 circulation response to abrupt CO2 forcing in the southern hemisphere: seasonality and
781 the role of the stratosphere. Journal of Climate, 30(21), 8497-8515, doi: 10.1175/JCLI-D-
782 16-0849.1

783 Gu, K., H. K. Tony Ng, M. L. Tang, and W. R Schucany (2008) Testing the Ratio of Two
784 Poisson Rates. Biometrical Journal: Journal of Mathematical Methods in Biosciences 50,
785 283–98.

786 Guo, H. and coauthors (2018) NOAA-GFDL GFDL-CM4 model output. Version 20190718.
787 Earth System Grid Federation. https://doi.org/10.22033/ESGF/CMIP6.1402

788 Hardiman, S. C., Butchart, N., Charlton-Perez, A. J., Shaw, T. A., Akiyoshi, H., Baumgaertner,
789 A., et al. (2011). Improved predictability of the troposphere using stratospheric final
790 warmings. Journal of Geophysical Research, 116, D18113,
791 https://doi.org/10.1029/2011JD015914

792 Harvey, B. J., L. C. Shaffrey, and T. J. Woollings (2013), Equator-to-pole temperature
793 differences and the extra-tropical storm track responses of the CMIP5 climate models,
794 Clim. Dyn., doi:10.1007/s00382-013-1883-9.

795 Hawkins, E. and R. Sutton (2012) Time of Emergence of Climate Signals, Geophys. Res. Lett.,
796 39.

797 Held, I.M., and coauthors (2019) Structure and Performance of GFDL's CM4.0 Climate Model,
798 Journal of Advances in Modeling Earth System, https://doi.org/10.1029/2019MS001829.

799 Hendon H., D. W. J. Thompson, E.-P. Lim, A. H. Butler, P. A. Newman, L. Coy, A. Scaife, I.
800 Polichtchouk, R. S. Gerrard, T. G. Shepherd and H. Nakamura (2019), Nature, 573, 496,
801 doi: doi: 10.1038/d41586-019-02858-0

802 Hitchcock, P., T. G. Shepherd, and G. L. Manney (2013) Statistical characterization of Arctic
803 polar-night jet oscillation events, J. Climate, 26, 2096-2116.

804 Hu, J., R. Ren and H. Xu (2014) Occurrence of winter stratospheric sudden warming events and
805 the seasonal timing of spring stratospheric final warming, J. Climate, 71, 2319-2334.

806 Huffman, M. (1984), An Improved Approximate Two-Sample Poisson Test. J. Roy Stat. Soc.:
807 Series C (Applied Statistics) 33 (2), 224–26.

808 Karpechko, A. Y. and E. Manzini (2012) Stratospheric influence on tropospheric climate change
809 in the Northern Hemisphere. J. Geophys. Res. 117, D05133, DOI
810 10.1029/2011JD017036.

811 Kelleher, M., B. Ayarzagüena and J. Screen (2019): Inter-seasonal connections between the
812 timing of the stratospheric final warming and Arctic sea ice, J. Climate,
813 https://doi.org/10.1175/JCLI-D-19-0064.1.

814 Kidston, J., A. A. Scaife, S. C. Hardiman, D. M. Mitchell, N. Butchart, M. P. Baldwin and L- J.
815 Gray (2015) Stratospheric influence on tropospheric jet streams, storm tracks and surface
816 weather, Nat. Geos., 8, 433-440.

817 Kim, J., Son, S.-W., Gerber, E. P., and Park, H.-S. (2017) Defining sudden stratospheric
818 warming in climate models: Accounting for biases in model climatologies, J. Clim., 30,
819 5529–5546.

820 Kobayashi, S., Ota, Y., Harada, Y., Ebita, A., Moriya, M., Onoda, H., Onogi, K., Kamahori, H.,
821 Kobayashi, C., Endo, H., Miyaoka, K., and Takahashi, K. (2015): The JRA-55 reanalysis:
822 General specifications and basic characteristics, J. Meteor. Soc. Jpn., 93, 5–48.

823 Kodera, K., K. Matthes, K. Shibata, U. Langematz, and Y. Kuroda (2003), Solar impact on the
824 lower mesospheric subtropical jet: A comparative study with general circulation model
825 simulations, Geophys. Res. Lett., 30(6), 1315, doi:10.1029/ 2002GL016124.

826 Krüger, K., B. Naujokat, and K. Labitzke (2005) The Unusual Midwinter Warming in the
827 Southern Hemisphere Stratosphere 2002: A Comparison to Northern Hemisphere
828 Phenomena, Journal of Climate, 62, 603-613.

829 Kuhlbrodt, T., Jones, C. G., Sellar, A.,Storkey, D., Blockley, E., Stringer, M., et al. (2018). The
830 low-resolution version of HadGEM3 GC3.1: Development and evaluation for global
831 climate. Journal of Advances in Modeling Earth Systems, 10, 2865–2888.
832 https://doi.org/10.1029/2018MS001370.

833 Kushner, P.J., and L.M. Polvani (2004). Stratosphere-troposphere coupling in a relatively simple
834 AGCM: The role of eddies. J. Climate, 17, 629-639.

835 Kushner, P.J., and L.M. Polvani (2005). A very large, spontaneous stratospheric sudden warming
836 in a simple AGCM: A prototype for the Southern Hemisphere warming of 2002? J.
837 Atmos. Sci., 62, 890-897.

838 Li, Q., H.-F. Graf and M. A. Giorgetta (2007) Stationary planetary wave propagation in the
839 Northern Hemisphere winter – climatological analysis of the refractive index,
840 Atmospheric Chemistry and Physics, 7, 183-200.

Mahfouf, J. F., D. Cariolle, J.-F. Royer, J.-F Geleyn and B. Timbal (1994) Response of the Météo-France climate model to changes in CO2 and sea surface temperature, Clim. Dyn. 9, 345-362.

Mailier, P. J, D. B Stephenson, C. AT Ferro, and K. I Hodges (2006) Serial Clustering of Extratropical Cyclones, Mon. Wea. Rev. 134 (8): 2224–40.

Manabe, S. and R. T. Wetherland (1967) Thermal equilibrium of the atmosphere with a given distribution of relative humidity, J. Atmos. Sci, 24, 241-259.

Manzini, E., and coauthors (2014) Northern winter climate change: Assessment of uncertainty in CMIP5 projections related to stratosphere-troposphere coupling, J. Geophys. Res. Atmos., 119, 7979-7998, doi:10.1002/2013JD021403.

McLandress, C., and T. G. Shepherd (2009), Impact of climate change on stratospheric sudden warmings as simulated by the Canadian Middle Atmosphere Model, J. Clim., 22, 5449–5463, doi:10.1175/ 2009JCLI3069.1

McLandress, C., A. I Jonsson, D. A. Plummer, M. C. Reader, J. F. Scinocca, T. G. Shepherd (2010), Separating the dynamical effects of climate change and ozone depletion. Part I: Southern Hemisphere stratosphere, J. Climate, 23, 5002-5020.

Meinshausen, M. and coauthors (2017) Historical greenhouse gas concentrations for climate modelling (CMIP6), Geosci. Model Dev., 10, 2057-2116, doi:10.5194/gmd-10-2057-2017.

Mitchell, D. M., Osprey, S. M., Gray, L. J., Butchart, N., Hardiman, S. C., Charlton-Perez, A. J., and Watson, P. (2012a) The effect of climate change on the variability of the Northern Hemisphere stratospheric polar vortex, J. Atmos. Sci., 69, 2608–2618, 2012a.

Mitchell, D. M., Charlton-Perez, A. J., Gray, L. J., Akiyoshi, H., Butchart, N., Hardiman, S. C., Morgenstern, O., Nakamura, T., Rozanov, E., Shibata, K., Smale, D., and Yamashita, Y. (2012b) The nature of Arctic polar vortices in chemistry-climate models, Q. J. Roy. Meteor. Soc., 138, 1681–1691.

NASA Goddard Institute for Space Studies (NASA/GISS) (2018). NASA-GISS GISS-E2.1G model output prepared for CMIP6 CMIP piControl. Version 20191120.Earth System Grid Federation. https://doi.org/10.22033/ESGF/CMIP6.7380

Oberländer-Hayn, S., S. Meul, U. Langematz, J. Abalichin and F. Haenel (2015) A chemistry-climate model study of past changes in the Brewer-Dobson circulation, Journal of Geophysical Research: Atmospheres, 120, 6742-6757.

Polvani, L.M., Sun, L., A.H. Butler, J.H. Richter, and C. Deser (2017), Distinguishing stratospheric sudden warmings from ENSO as key drivers of wintertime climate variability over the North Atlantic and Eurasia, J. Climate, 30, 1959-1969, doi: 10.1175/JCLI-D-16-0277.1.

Rind, D., R. Suozzo, N. K. Balachandran, and M. J. Prather (1990) Climate change and the middle atmosphere. Part I: The doubled CO2 climate, J. Atmos. Sci., 47, 475-494.

Rind D., D. Shindell, P. Lonergan, and N. K. Balachandran (1998) Climate change and the middle atmosphere. Part III: The doubled CO2 climate revisited, J. Clim., 11, 876-894.

881 Roberts, M. (2017). MOHC HadGEM3-GC31-LL model output prepared for CMIP6. Version
882 20190723.Earth System Grid Federation. https://doi.org/10.22033/ESGF/CMIP6.1901

883 Scaife, A., et al. (2012), Climate change projections and stratosphere–troposphere interaction,
884 Clim. Dyn., doi:10.1007/s00382-011-1080-7.

885 Schoeberl, M. R., and D. L. Hartmann (1991) The dynamics of the stratospheric polar vortex and
886 its relation to springtime ozone depletions, Science, 251, 46-52.

887 Sellers, K. F, and D. S Morris (2017) Underdispersion Models: Models That Are 'Under the
888 Radar', Communications in Statistics-Theory and Methods 46 (24), 12075–12086.

889 Séférian, R. (2018) CNRM-CERFACS CNRM-ESM2-1 model output prepared for CMIP6
890 CMIP for experiment piControl-spinup. Version 20180423. Earth System Grid
891 Federation. https://doi.org/10.22033/ESGF/CMIP6.4169

892 Séférian, R. and coauthors (2019) Evaluation of CNRM Earth-System model, CNRM-ESM2-1:
893 role of Earth system processes in present-day and future climate, Journal of Advances in
894 Modeling Earth Systems, https://doi.org/10.1029/2019MS001791.

895 Shepherd T.G. and C. S. McLandress (2011) A robust mechanism for strengthening of the
896 Brewer–Dobson circulation in response to climate change: Critical-layer control of
897 subtropical wave breaking, J. Atmos. Sci., 69, 784-797, doi: 10.1175/2010JAS3608.1

898 Song, Y. and W. A. Robinson (2004) Dynamical mechanisms for stratospheric influences on the
899 troposphere, J. Atmos. Sci., 61,1711-1725.

900 Swart, N. C., Cole, J. N. S., Kharin, V. V., Lazare, M., Scinocca, J. F., Gillett, N. P., Anstey, J.,
901 Arora, V., Christian, J. R., Hanna, S., Jiao, Y., Lee, W. G., Majaess, F., Saenko, O. A.,
902 Seiler, C., Seinen, C., Shao, A., Sigmond, M., Solheim, L., von Salzen, K., Yang, D., and
903 Winter, B. (2019a) The Canadian Earth System Model version 5 (CanESM5.0.3), Geosci.
904 Model Dev., 12, 4823–4873, https://doi.org/10.5194/gmd-12-4823-2019.

905 Swart, Neil Cameron; Cole, Jason N.S.; Kharin, Viatcheslav V.; Lazare, Mike; Scinocca, John
906 F.; Gillett, Nathan P.; Anstey, James; Arora, Vivek; Christian, James R.; Jiao, Yanjun;
907 Lee, Warren G.; Majaess, Fouad; Saenko, Oleg A.; Seiler, Christian; Seinen, Clint; Shao,
908 Andrew; Solheim, Larry; von Salzen, Knut; Yang, Duo; Winter, Barbara; Sigmond,
909 Michael (2019). CCCma CanESM5 model output prepared for CMIP6 CMIP piControl.
910 Version 20190730. Earth System Grid Federation.
911 https://doi.org/10.22033/ESGF/CMIP6.3673

912 Taguchi, M. (2017) A study of different frequencies of major stratospheric sudden warmings in
913 CMIP5 historical simulations, Journal of Geophysical Research: Atmospheres, 122,
914 5144-5156, doi: 10.1002/2016JD025826.

915 Tang, Y. and coauthors (2019). MOHC UKESM1.0-LL model output prepared for CMIP6 CMIP
916 piControl. Version 20190904. Earth System Grid Federation.
917 https://doi.org/10.22033/ESGF/CMIP6.6298

918 Tatebe, H. and Watanabe, M. (2018). MIROC MIROC6 model output prepared for CMIP6
919 CMIP piControl. Version 20190903.Earth System Grid Federation.
920 https://doi.org/10.22033/ESGF/CMIP6.5711

Tatebe, H., and coauthors (2019) Description and basic evaluation of simulated mean state, internal variability, and climate sensitivity in MIROC6, Geosci. Model Dev., 12, 2727–2765, https://doi.org/10.5194/gmd-12-2727-2019.

Volodin, E. M., Mortikov, E. V., Kostrykin, S. V., Galin, V. Y., Lykossov, V. N., Gritsun, A. S., Diansky, N. A., Gusev, A. V., and Iakovlev, N. G. (2017) Simulation of the present day climate with the climate model INMCM5, Clim. Dyn., 49, 3715, https://doi.org/10.1007/s00382-017-3539-7

Wilks, Daniel S. (2011). *Statistical Methods in the Atmospheric Sciences*. Vol. 100. Academic press.

Williams, K., Copsey, D., Blockley, E., Bodas-Salcedo, A., Calvert, D., Comer, R., Davis, P., Graham, T., Hewitt, H., & Hill, R. (2018). The Met Office global coupled model 3.0 and 3.1 (GC3. 0 and GC3. 1) configurations. Journal of Advances in Modeling Earth Systems, 10(2), 357–380.

Wu, Y., Simpson, I. R. and Seager, R. (2019) Inter-model spread in the Northern Hemisphere stratospheric polar vortex response to climate change in the CMIP5 models, Geophys. Res. Lett., In Press.

Yukimoto, S. and coauthors (2019). MRI MRI-ESM2.0 model output prepared for CMIP6 CMIP. Version 20190726.Earth System Grid Federation. https://doi.org/10.22033/ESGF/CMIP6.621

Yukimoto, S. and coauthors (2019) The Meteorological Research Institute Earth System Model Version 2.0, MRI-ESM2.0: Description and Basic Evaluation of the Physical Component, Journal of Meteorological Society of Japan, 97(5),931−965, doi:10.2151/jmsj.2019-051